Appendix C

BOUNDARY LAYER PROFILE MEASUREMENTS IN THE ELECTRODE WALL OF A COMBUSTION DRIVEN MHD CHANNEL*

R. K. James and C. H. Kruger

95D 3102

High Temperature Gasdynamics Laboratory

Department of Mechanical Engineering

Stanford University

Presented at the

17th Symposium on Engineering Aspects of Magnetohydrodynamics

March 27-29, 1978

Stanford University

DISCLAIMER

BOUNDARY LAYER PROFILE MEASUREMENTS IN THE ELECTRODE WALL OF A COMBUSTION DRIVEN MHD CHANNEL*

R. K. James and C. H. Kruger
High Temperature Gasdynamics Laboratory
Stanford University

Abstract

Profiles of temperature and electron number density were measured in the electrode wall boundary layer of the Stanford M-2 MHD channel with applied electric field. Results were obtained for two flow conditions, and several electrical conditions. Calculations of profiles using a boundary layer computer program were made. Measured temperature profiles with no current showed some discrepancies with the theory, but generally the agreement between theory and experiment was adequate. The Joule heating of the plasma caused a significant increase in the measured temperature profiles. Good agreement was obtained between calculated and measured profiles that included the effect of Joule heating. Some electron number density non-equilibrium near the wall was apparently observed, although the amount of non-equilibrium was less than predicted. At high local current densities, measurements show the electron number density profile to be relatively flat near the wall at current densities where the anode voltage drop appears to indicate that a current constriction is occurring.

Introduction

The accurate prediction of boundary layer loss mechanisms such as electrode voltage drop and wall heat transfer is important to the design of MHD generators. Effects such as variable properties, wall roughness, turbulence, non-equilibrium, and electrical interactions present modeling difficulties which require that experimental verification be done of the theories that attempt to predict the boundary layer transport. Measurements of the actual boundary layer profiles are particularly important in verifying the details of the boundary layer models.

This is an experimental investigation of three effects that have been predicted to occur in MHD flows, and have possibly important consequences in the prediction of wall heat transfer and electrode voltage drop. These effects are 1) electron non-equilibrium near the electrode due to the effect of finite rate recombination kinetics, 2) Joule heating, and 3) current constriction at high local current densities. Daily[1] predicted that electron non-equilibrium would occur in the boundary layer of an MHD generator, and made measurements of N_e in an MHD generator, but did not obtain data in regions of the boundary layer where non-equilibrium was expected. Joule heating has also been studied theoretically in MHD boundary layers, and is predicted to be important in generators with high Hall parameters.[2] Current constrictions in the boundary layer have been predicted by Oliver[3] to occur under certain conditions in MHD boundary layers. Such constrictions could lead to high local heating rates on the electrode surface, as well as have significant effects on the electrode voltage drop.

To investigate these effects, experiments were run where electron number density profiles, temperature profiles, and electrode voltage drops were measured in the electrode wall boundary layer of the Stanford M-2 MHD channel with an applied electric field. Particular emphasis was placed on measuring as close to the electrode surface as possible. The final measurements have a spatial resolution of 0.3 mm, with the first measured point in the boundary layer at typically 0.4 mm. Experimental conditions were chosen where the effects of interest would be important and accessible to the plasma diagnostics.

Experimental Procedures

The experiments were run in the Stanford M-2 facility. Figure 1 shows a diagram of the experimental setup. Alcohol seeded with KOH to give a 1% K concentration is burned with oxygen and nitrogen diluent. The plasma passes into a plenum where combustion is completed, then into a run-in section and the MHD channel. The MHD channel had 13 electrode pairs. The run-in section was used before the MHD channel to enhance boundary layer growth. Spectroscopic measurements were made on the last electrode, giving a total length for boundary layer development of 1.09 meters. The channel had a height of 10 cm and a width of 3.1 cm. Optical access to the channel was provided by two 5 cm high by 2 cm wide open ports in the sidewall of the channel.

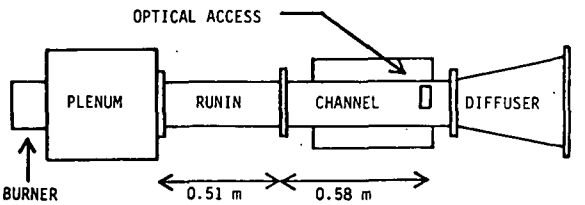

Fig. 1. Experimental Apparatus

Although the boundary layer phenomena under investigation in these experiments are affected by the presence of the magnetic field, they depend principally on the local current density. As the magnet greatly compounds the optical access problems, no magnetic field was used in these experiments. Battery banks provided power for the electrodes.

The experiments consisted of three separate phases. In the first phase, the emphasis was on measuring the degree of non-equilibrium in the electron number density near the wall. Eight minute scans of the boundary layer were performed using two different spectral lines in the electron number density diagnostic. The temperature profile was measured, and electrode voltage drops were measured at low current density. In the second phase, the emphasis was on the effect of

*Supported by U.S. Department of Energy under Contract EX 76-C-01-2341.

Joule heating on the temperature profiles. A reference temperature profile was measured, and then another profile measurement was performed while the current was on. No current was run on the last electrode in order to insure that electron temperature elevation did not exist where the measurements were being taken, as this can lead to difficulties in interpreting the temperature data. The current was chosen to be high enough to cause a significant effect on the measured temperature profile. Electron number density profiles were then measured with and without current. In the final phase of the experiments, single electrode pairs were run with a high current density, while in one case voltage drops were measured, and in another the electron number density profile. This final phase examined the stability of the boundary layer with a high local current density.

Diagnostics

The spectroscopic diagnostics used in the experiments consisted of a temperature measurement system using a sodium line reversal method, and an electron number density measurement system using an absolute intensity measurement of high-lying energy states in the potassium atom. The diagnostics are similar in principle to those used by Daily in ref. 1, although significant technical improvements have been made. Improvements in the optical hardware and alignment procedures have increased the spatial resolution near the wall in both the temperature and electron number density measurements. A digital data acquisition and signal processing system has significantly reduced the noise in the N_e measurement. These improvements allow measurements to be made of N_e very near the wall where non-equilibrium has been predicted to occur.

The temperature diagnostic relies on Kirchoff's law, which states that the emissivity and absorptivity of a gas at a given wavelength are equal. The measurement must be made in a region of the spectrum where the optical depth of the gas is approximately 0.1 to 1.0. The spectral region very near the sodium D lines at 5900 Å provides a suitable optical depth when the plasma is seeded with a small amount of sodium. A gas temperature determination is made by obtaining four radiation intensity signals from the plasma. The four required signals are obtained by recording the intensity of radiation from the plasma with and without a calibrated lamp filament focused in the plasma, at two different optical depths. The lamp on and off conditions are obtained by chopping the lamp and using a simple digital processing scheme to demodulate the signal into the two required signals. Although in principle one of the optical depths could be chosen to be zero, and thus with no gas interaction the measurement could be taken before the experiment, in practice small drift problems in the light collection system make it more accurate to obtain the four signals during the experiment as close together in time as practical. The required variation in optical depth is accomplished by varying the wavelength.

To calculate the temperature, express the four PMT signals P_1, P_2, P_3, P_4 in terms of optical depths τ_A, τ_B, lamp blackbody temperature T_b, plasma temperature T_p, Planck function B_ν, wavelengths λ_A, λ_B, and optics calibration factors K_A, K_B.

$$P_1 = K_A \left[(1 - e^{-\tau_A}) B_\nu(T_p,\lambda_A) + e^{-\tau_A} B_\nu(T_b,\lambda_A) \right] \quad \text{(lamp + emission)}$$

$$P_2 = K_A \left[(1 - e^{-\tau_A}) B_\nu(T_p,\lambda_A) \right] \quad \text{(emission only)}$$

$$P_3 = K_B \left[(1 - e^{-\tau_B}) B_\nu(T_p,\lambda_B) + e^{-\tau_B} B_\nu(T_b,\lambda_B) \right] \quad \text{(lamp + emission)}$$

$$P_4 = K_B \left[(1 - e^{-\tau_B}) B_\nu(T_p,\lambda_B) \right] \quad \text{(emission only)}$$

These four equations plus a calibration curve of P vs. λ for the optical system can be solved to yield the 5 unknowns K_A, K_B, τ_A, τ_B, and T_p, though the expression is long and requires iteration. If λ_A is very near λ_B such that $K_A = K_B$ and $B_\nu(T,\lambda_A) = B_\nu(T,\lambda_B)$, then a simple solution for the temperature can be derived, giving

$$T_p = C/\left[C/T_b + \ell n\left(1 + \frac{P_1 - P_3}{P_4 - P_2} \right) \right]$$

where $C = hc/\lambda k = 24420$ K for $\lambda = 5890$ Å. This formula is similar to that used by Vasil'eva for core temperature measurements in the Soviet U-25 MHD facility.[4] Note that this equation involves only differences of signals, so a constant DC bias in the signal processing electronics can be tolerated without sacrificing accuracy in the temperature determination.

The electron number density diagnostic relies on the Saha equation:

$$N_e^2 = N_k \frac{g_i^+}{g_k} \left(\frac{2\pi m_e k T}{h^2} \right)^{3/2} \exp(-\varepsilon_{k\lambda}/kT)$$

where g_i^+ and g_k are the ion and excited state degeneracies, and $\varepsilon_{k\lambda}$ is the energy difference between the excited state and the ionization limit. This equation relates the electron number density N_e to the number density N_k of excited states in the potassium atom. The number densities of these excited states are measured by performing an absolute intensity measurement on radiation emitted from upper to lower state transitions. The lower state is chosen to be a non-ground state so as to minimize reabsorption of the emitted radiation. The upper state is chosen to be as close to the ionization limit of the potassium atom as is practical, as the high-lying states of the potassium atom will be in equilibrium with the free electrons even when a degree of non-equilibrium exists between the free electrons and the potassium ground state. In the present experiments, 6D-4P (5360 Å), 7D-4P (5112 Å) and 8D-4P (4965 Å) transitions are used. The following equation relates the population of the upper state to the measured absolute intensity I in the plasma:

$$I = h\nu L \frac{A_{k\ell}}{4\pi} N_k$$

where L is the path length of the plasma. This equation relies on the Einstein coefficient $A_{k\ell}$, a fundamental constant of the potassium atom which is only known to ± 50% for the desired transitions. This limits the absolute accuracy of the diagnostic to ± 25%. Because of this absolute accuracy limitation, the values of N_e

presented in this paper have been corrected by a factor to make the measured core N_e match the equilibrium N_e based on the measured core temperature. The raw measured values are typically multiplied by about 1.15 to yield the final N_e value.

Figure 2 shows a diagram of the optical system. The same basic system is used for both the temperature and electron number density measurements. A calibrated tungsten strip lamp located on one side of the channel is imaged into the plasma to serve as a calibration source for both the temperature and N_e measurements. The lamp radiation is chopped to give, for the temperature measurement, an emission only and an emission plus transmission signal, while for the electron number density the chopper provides DC rejection during the system calibration. A scanning mirror is placed at the focal point of the field lens to allow a parallel scanning of the boundary layer. The region near the wall is scanned more slowly than the core regions to improve signal quality near the wall. The SPEX 0.5 meter focal length monochromator has an internal spectral scanning mirror, which is used during the electron number density measurements to repetitively scan a region of about 5.0 Å centered on the desired spectral line.

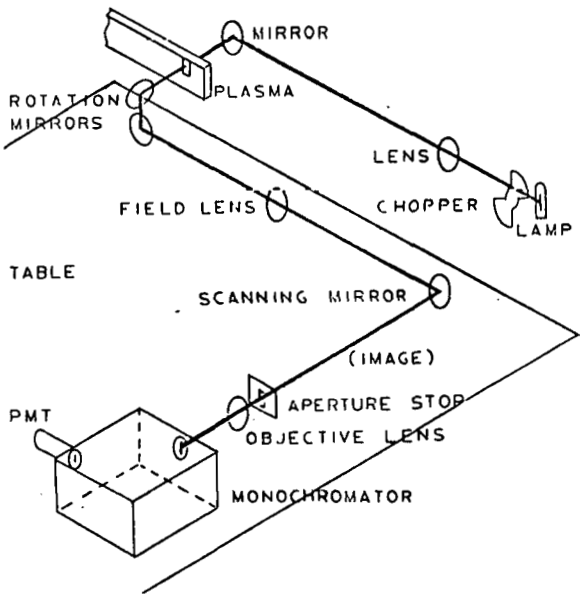

Fig. 2. Boundary Layer Optics

An estimation procedure was developed to recover the weak signals that are encountered in the electron number density measurements. The desired quantity is the integrated line intensity I, which is:

$$I = \int_{\nu_o-\Delta}^{\nu_o+\Delta} I_\nu(\nu)d\nu$$

The integration is performed about a region 2Δ centered on the line center ν_o, where Δ is chosen to include only the line of interest and not adjacent lines. The photomultiplier signal has significant background noise due to continuum radiation and collection noise. In order to reduce the effect of this background noise to a minimum, it is necessary to keep the spectral bandpass of the monochromator to a minimum. This precludes operating the monochromator such that, by increasing the bandpass of the monochromator, the slits perform the required spectral integration, as this increase in bandpass causes a proportional increase in noise, while the signal strength remains constant. To overcome this problem, the monochromator was run with narrow slits and a digital signal processing scheme was developed to determine the value of the line intensity. As, relative to the monochromator resolution, the lines being observed are narrow, the observed shape of the line is due principally to the monochromator instrument broadening, which remains constant throughout the boundary layer scan. It is possible to take advantage of this fact in a signal processing scheme. The observed line shape is expressed in a unity-integral function $f(\lambda)$, which is obtained by averaging and normalizing the spectral data for the entire boundary layer. The signal P received from the PMT is assumed to consist of y-dependent noise n and line intensity s:

$$P(\lambda,y) = n(y) + s(y)f(\lambda),$$

At a given spatial location, N (approximately 400) points of varying wavelength λ_i are obtained. Using these points, the least squares fit to n and s is made, giving:

$$D = N \Sigma f_i^2 - (\Sigma f_i)^2$$

$$n = \frac{1}{D}\left[\Sigma P_i \Sigma f_i^2 - \Sigma P_i f_i \Sigma f_i\right]$$

$$s = \frac{1}{D}\left[N \Sigma P_i f_i - \Sigma f_i \Sigma P_i\right]$$

This scheme gives a significant improvement in signal quality over other schemes that have been used such as straightforward integration of the spectral data or using the monochromator with a wide exit slit to perform the spectral integration.

A boundary layer correction must be applied to the data to account for the effect of the sidewall boundary layers on the diagnostic measurements. The correction procedure follows Daily[5] for the temperature profile. For the N_e measurement, the following procedure is used. Using a one-seventh power temperature profile, the equilibrium excited state population N_k is calculated. A path integral of the calculated N_k profile is performed, and electron number density is calculated based on the integrated and core N_k values. The ratio of these two calculated electron number densities is then used to correct the measured N_e to yield the core value.

Boundary Layer Modeling

Calculations from a modified version of a boundary layer program originally developed by Daily[1] were used to interpret the experimental data. The following equations describe the boundary layer model:

Continuity:

$$\frac{\partial\overline{\rho u}}{\partial x} + \frac{\partial\overline{\rho v}}{\partial y} + \frac{\partial\overline{\rho w}}{\partial z} = 0 ,$$

Momentum:

$$\overline{\rho u}\frac{\partial\overline{u}}{\partial x} + \overline{\rho v}\frac{\partial\overline{u}}{\partial y} = \frac{\partial}{\partial y}\left((\mu + \overline{\rho\varepsilon_m})\frac{\partial\overline{u}}{\partial y}\right) - \frac{\partial p}{\partial x} ,$$

Energy:

$$\overline{\rho u}\frac{\partial \overline{H}}{\partial x} + \overline{\rho v}\frac{\partial \overline{H}}{\partial y} = \frac{\partial}{\partial y}\left(\frac{\mu}{Pr}\left(1 + \frac{\epsilon_D}{\alpha}\right)\frac{\partial \overline{H}}{\partial y}\right) + \frac{1}{2}\frac{\partial}{\partial y}\left((\mu + \overline{\rho}\epsilon_m)\left(1 - \frac{1}{Pr}\right)\frac{\partial \overline{u}^2}{\partial y}\right) + \vec{J}\cdot\vec{E} ,$$

Electron-Ion Continuity:

$$\overline{\rho u}\frac{\partial \overline{C_e}}{\partial x} + \overline{\rho v}\frac{\partial \overline{C_e}}{\partial y} = \frac{\partial}{\partial y}\left(\overline{\rho}\,(D_a + \epsilon_D)\frac{\partial \overline{C_e}}{\partial y}\right) + \dot{R}_e ,$$

where the electron and ion continuity equations have been combined to eliminate the electric field and D_a is the ambipolar diffusion coefficient, $\overline{C_e}$ the average electron concentration, and $\overline{H}$ the average total enthalpy. These equations, plus an equation of state and the appropriate initial boundary conditions, provide a complete description of the problem as considered.

The recombination coefficient for the electrons was obtained from Curry[6], who presented a recombination coefficient which was corrected for use in combustion gases:

$$\alpha = 2.519 \times 10^{-33}\, N_e(M^{-3})\, e^{-2.98 \times 10^{-3}\, T\,(°K)} \quad (m^3/sec)$$

The source term for the electron ion continuity equation becomes

$$\dot{R}_e = M_e\dot{N}_e = M_e\,\alpha\left(N_e^{*2} - N_e^2\right) ,$$

where the star indicates that the equilibrium value of N_e is to be used.

A mixing length model for the turbulence from the STAN5 boundary layer program was used[7]. The roughness model suggested by Healzer, et al.[8] was added to the STAN5 model.

Results and Discussion

Figure 3 shows a plot of a temperature profile, with a corresponding calculated profile, for zero current conditions with $N_2/O_2 = 1.0$, and a mass flow of 0.181 kg/sec, giving a free stream velocity of 450 m/sec. The calculated profile uses standard values of the turbulence parameters, with a sand grain roughness of 2.0 mm. The match of theory to measurement is good, although discrepancies are observed. The calculated profile with roughness included provides a better fit to the data than one without roughness, particularly for the points very near the wall, as the slope of the predicted profile without roughness is too great near the wall. The sandgrain roughness value used in the calculation was selected to give the best fit to the data, however the value used seems to be excessively large. Sonju[9] made measurements of friction factors in a modified version of the Stanford M-2 channel, and reported that the measured friction factors matched friction factor correlations for a roughness size of about 0.1 mm. The electrode wall observed in the present experiment should have a larger roughness than the brick walls used by Sonju, but a roughness of 0.5 mm seems more reasonable than the 2.0 mm roughness which seems to fit the data better. Daily[1] and Maxwell[2] have suggested that recirculation effects may be important in MHD channel flows, and so a recirculation model might improve the match of data to theory. Another possible source of the discrepancies is the effect of the hot upstream brick, which could give rise to a variation in the temperature profile very near the wall which is not adequately modeled by the present temperature boundary condition, which averages the wall parameters over the brick and electrode surfaces. Further work is planned to determine the source of the discrepancies noted between data and theory.

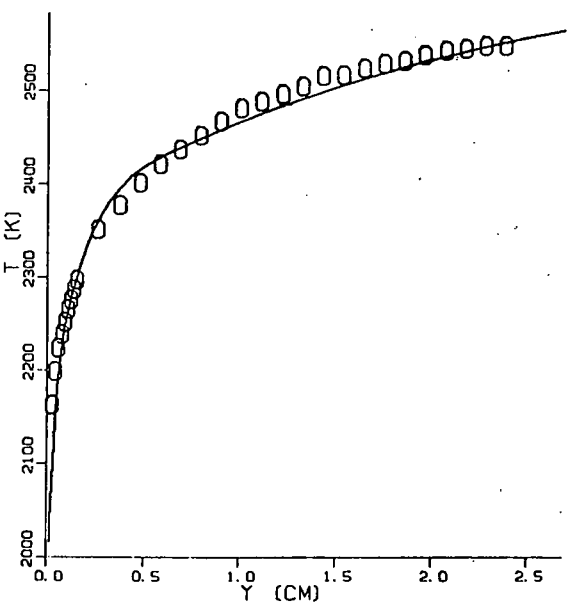

Fig. 3. Experimental and Theoretical Temperature Profiles, $N_2/O_2 = 1.0$, u = 450 m/s.

Figure 4 is a plot of temperature profiles with $N_2/O_2 = 0.5$, and a mass flow of 0.136 kg/sec, giving a free stream velocity of about 350 m/s. The run with current had an average current density of 1.54 amps/cm^2 over the 45.7 cm powered length of the channel. These profiles demonstrate the effect of Joule heating on the temperature

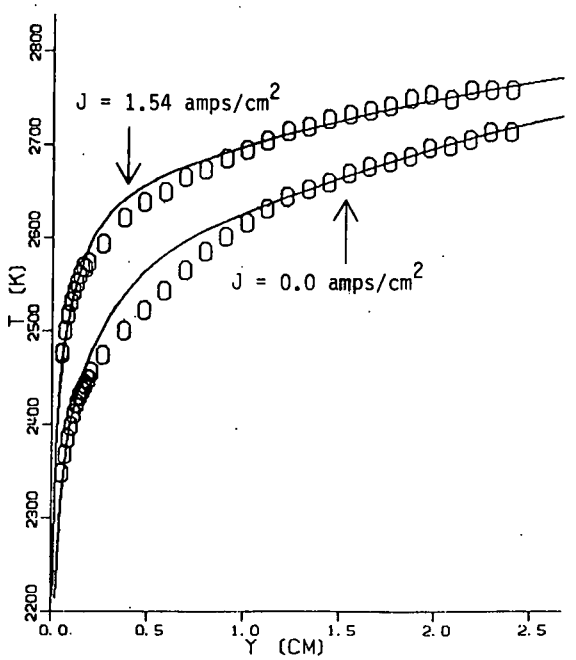

Fig. 4. Experimental and Theoretical Temperature Profiles With and Without Current, $N_2/O_2 = 0.5$, u = 350 m/s.

profile. The solid lines show calculations of the profiles, using the roughness parameter discussed above. The profile with no current shows small discrepancies similar to those in the previously discussed profile. The effect of the Joule heating on the temperature profile is predicted very well by the theory. Figure 5 shows the calculated Stanton number for the runs of Figure 4. At the beginning of the electrode section, St jumps upward due to the lower temperature of the electrodes relative to the upstream bricks. The Joule heating causes a 15% increase in Stanton number at the end of the channel. In a full scale generator, the effect of Joule heating would be decreased by the higher velocities and higher wall temperatures, but increased at high Hall parameters by the resulting current concentrations.

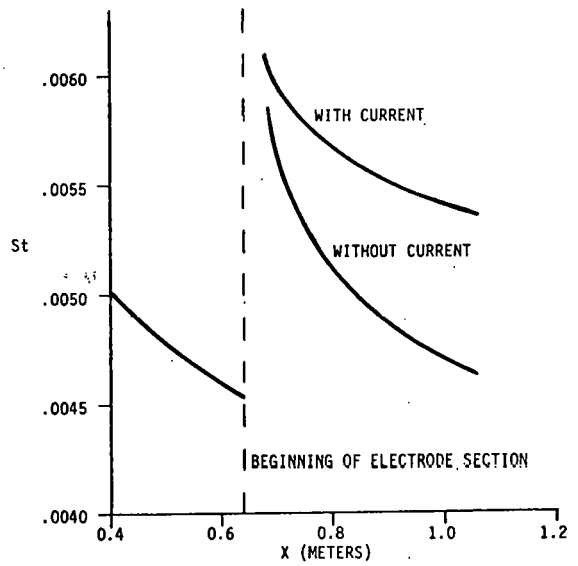

Fig. 5. Calculated Effect of Joule Heating on Stanton Number, N_2/O_2 = 0.5, u = 350 m/s.

Figure 6 is a plot of measured electron number density at zero current along with the equilibrium electron number density based on the measured temperature, and calculated equilibrium and non-equilibrium profiles using a 2.0 mm roughness size. The conditions of this run are identical to those of Figure 3. The comparison of measurement and theory is good, but since away from the wall the electron number density is expected to be equal to the equilibrium number density, discrepancies in this figure are a result of the previously discussed discrepancies between the calculated and observed temperature profiles. Figure 7 is an expansion of Figure 6 very near the wall. Some non-equilibrium seems to appear very near the wall, but the non-equilibrium is not as much as was expected from the calculation. One possible explanation for the discrepancy is that the electron recombination coefficient used in the calculation underpredicted the recombination rate, thus giving rise to a too high predicted non-equilibrium near the wall. Such an error in the recombination rate could have important effects on the calculated electrode voltage drop, as the plasma resistance based on the calculated non-equilibrium profile was 60% of the resistance based on the equilibrium profile. As these experiments did not show very good agreement of measured

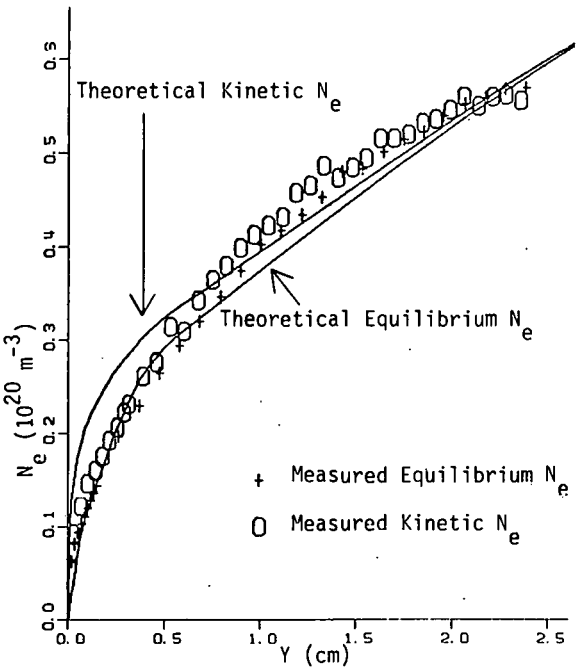

Fig. 6. Experimental and Theoretical N_e Profiles, N_2/O_2 = 1.0, u = 450 m/s.

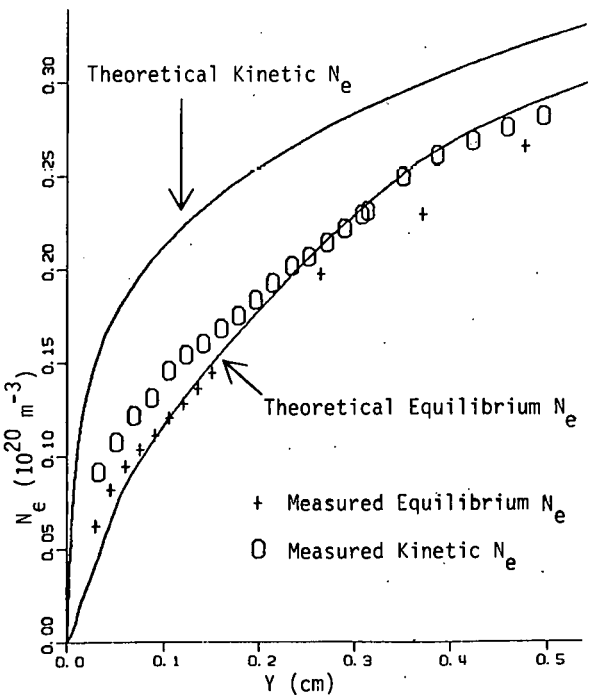

Fig. 7. Experimental and Theoretical N_e Profiles, Near the Wall, N_2/O_2 = 1.0, u = 450 m/s.

with predicted non-equilibrium, further work is indicated to establish the source of the discrepancies.

In the final phase of the experiments, high current densities were run in an attempt to simulate the plasma conditions with a local current concentration due to the Hall effect. Local current densities up to 14 amps/cm^2 were obtained by applying 720 volts of batteries to the electrode circuit. This phase of the experiments was

a preliminary study to determine if current constrictions would occur at high current densities, and to determine the value of the spectroscopic diagnostics in analyzing such behavior. These results are presented as empirical observations with no attempt at theoretical explanations. Movies of the electrode showed arcing through the edges of the upstream and downstream insulators as the current streamlines spread out due to the lack of guard electrodes, but no evidence of shorting to the channel walls or the adjacent electrodes was observed upon channel disassembly. The movies also did not show evidence of arc spots on the electrode surface, although with arcs occurring through the insulators, it was difficult to determine the existence of arcing into the plasma from the movies. Voltage drop measurements between the anode and a voltage probe located 7.5 mm from the electrode surface are shown in Figure 8. These results show that above a certain current density, the voltage drop begins to fall, suggesting that a transition from diffuse to constricted current transfer occurred. Electron number density data (using the 6D-4P transition) from another electrode for three runs at different current densities is shown in Figure 9. The field of view of the N_e diagnostic was increased for this run such that approximately the entire electrode surface was being observed by the diagnostic. The temperature was not measured in these runs, so the temperature required in the electron number density data reduction was obtained by assuming that N_k was in equilibrium with the ground state at the electron temperature. The electron number density in the cooler regions of the boundary layer begins to rise substantially near the same current density where the voltage drop began to fall on the other electrode. At higher current densities, the electron number density profile in the region accessible to the diagnostic appears to be almost flat. Deterioration of the wall had decreased spatial resolution such that only points farther than 2.0 mm from the wall could be observed. No evidence of intense arcing was seen in the regions viewed by the electron number density diagnostic, as arcing would be expected to cause a dramatic increase in electron number density, and observations of the raw spectroscopic data show no evidence of intense radiation from an arc being emitted from the plasma. The principal conclusions that can be drawn from this initial study of transverse stability are that there is some evidence from the voltage drop data of transition to constricted mode of current transfer at sufficiently high current densities, and at these current densities substantial elevation of N_e occurred in the boundary layer.

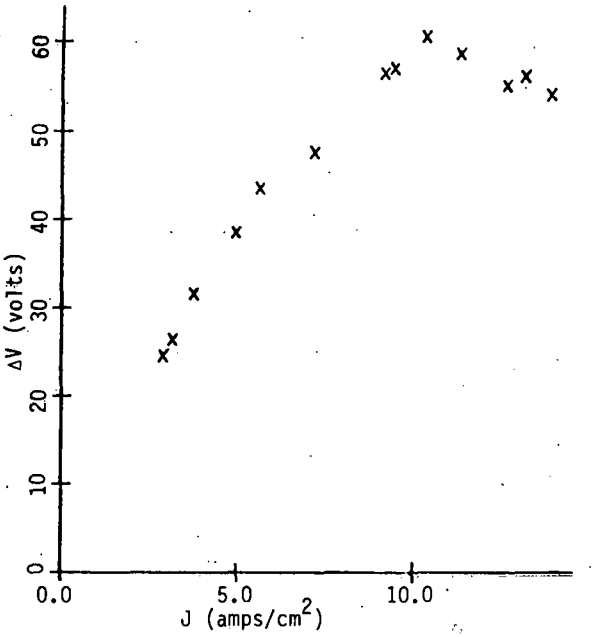

Fig. 8. Voltage Difference Between Anode and Voltage Probe Located 7.5 mm from the Surface. J based on electrode dimension.

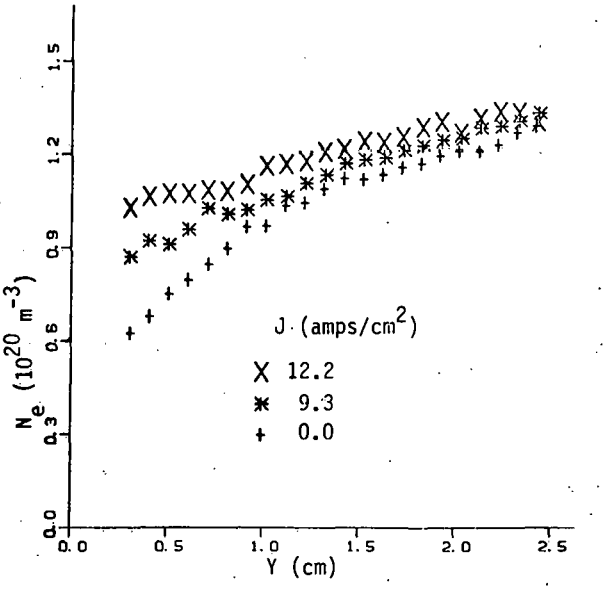

Fig. 9. Measured N_e at High Current Densities.

Summary

Measurements of electron number density and temperature profiles were made on the Stanford M-2 MHD channel. Temperature profiles with no current agreed with calculations from a boundary layer computer program, particularly in the slope of the profile near the wall, only when a roughness correction was included in the calculation. Measurements with current showed the effect of Joule heating on the temperature profiles. The theoretical predictions for the Joule heating agreed well with the experiment. Measurements of electron number density very near the wall did not show as much non-equilibrium as was expected from calculations. At local current densities of about 10.0 amps/cm^2, voltage drop measurements suggested that a transition from diffuse to constricted current transfer occurred. Electron number density profiles at these current densities were almost flat.

Acknowledgements

The authors gratefully acknowledge the technical assistance and guidance of Mr. Frank Levy and Mr. Philip Krug of the High Temperature Gasdynamics Laboratory. R. K. James acknowledges support from an NSF graduate fellowship.

References

1. Daily, J. W., C. H. Kruger, S. A. Self, R. H. Eustis, "Boundary Layer Profile Measurements in a Combustion Driven Generator," Sixth International Conference on Magnetohydrodynamic Electrical Power Generation, June 1975, also AIAA J. 14, August 1976, pp. 997-1005.

2. Maxwell, C. D., D. M. Markham, S. T. Demetriades, and D. A. Oliver, "Coupled Electrical and Fluid Calculations in the Cross Plane in Linear MHD Generators," Proceedings of the 16th Symposium on Engineering Aspects of MHD, Pittsburgh, Penn., May, 1977.

3. Oliver, D. A., "A Constricted Discharge in Magnetohydrodynamic Plasma," Proceedings of the 15th Symposium on Engineering Aspects of MHD, Philadelphia, Penn., May 1976.

4. Vasil'eva, I. A., V. V. Kirillov, I. A. Maksimov, G. P. Malyuzhonok, and B. B. Novosadov, "Measurement of a Plasma's Temperature by a Spectroscopic Method with Continuous Automatic Detection," High Temperature, 11, 4, pp. 838-845, July-August, 1973.

5. Daily, J. W. and C. H. Kruger, "Effect of Cold Boundary Layers on Spectroscopic Temperature Measurements in Combustion Gas Flows," AIAA 14th Aerospace Sciences Meeting, Paper #76-134, Washington, D.C., January 1976, also J. Quant. Spectros. Radiat. Transfer 17, 1977, pp. 327-338.

6. Curry, B. P., "Collisional Radiative Recombination in Hydrogen Plasmas and in Alkali Plasmas," Phys. Rev. A, 1, 1970, 166-176, and OCR Progress Report, August 16-September 15, 1973, STD Corp. Actual numerical values used in the calculations were obtained from the progress report.

7. Crawford, M. E. and W. M. Kays, "STAN5 - A Program for Numerical Computation of Two-Dimensional Internal/External Boundary Layer Flows," Report No. HMT-23, Mechanical Engineering Department, Stanford University, December 1975.

8. Healzer, J. M., R. J. Moffat, and W. M. Kays, "The Turbulent Boundary Layer on a Rough, Porous Plate: Experimental Heat Transfer With Uniform Blowing," Report HTM-18, Mechanical Engineering Department, Stanford University, May 1974.

9. Sonju, O. K. and C. H. Kruger, "Experiments on Hartmann Channel Flow in Plasmas," Phys. Fluids 12, 12 (Dec. 1969).